Journal of Alloys and Compounds 1045 (2025) 184763

Contents lists available at ScienceDirect

Journal of Alloys and Compounds

journal homepage: www.elsevier.com/locate/jalcom

Interplay between extended and point structural defects in BGaN/SiC epitaxial layers grown by MOCVD

C. Romanitan [a,1,*], J. Mickevičius [b,1], N. Djourelov [c], A.B. Serban [c], O. Brincoveanu [a], A. Kadys [b], T. Malinauskas [b], I. Mihalache [a], E.M. Pavelescu [a,d,**]

[a] National Institute for Research and Development in Microtechnologies, Erou Iancu Nicolae 126A, Voluntari 077190, Romania
[b] Institute of Photonics and Nanotechnology, Vilnius University, Saulėtekio al. 3, Vilnius LT-10257, Lithuania
[c] Extreme Light Infrastructure-Nuclear Physics (ELI-NP), 'Horia Hulubei' National R&D Institute for Physics and Nuclear Engineering (IFIN-HH), 30 Reactorului Street, Măgurele, Ilfov 077125, Romania
[d] Faculty of Electronics, Telecommunications and Information Technology, National University of Science and Technology POLITEHNICA Bucharest, Iuliu Maniu Avenue 1-3, Bucharest 061071, Romania

ARTICLE INFO

Keywords:
Boron gallium nitride
Reciprocal space maps
Threading dislocations
Point defects
Positron annihilation spectroscopy

ABSTRACT

Formation of point defects in BGaN/SiC epilayers grown by metal-organic chemical vapor deposition was investigated by positron annihilation spectroscopy in conjunction with X-ray diffraction, photoluminescence and scanning electron microscopy. The increase in the point defect density was associated with the introduction of boron atoms and manifested in the rising relative intensity of the defect-related photoluminescence band. An increase in boron content in the layer up to 3.4 % resulted in higher densities of both threading dislocations and point defects, and the interplay between different types of defects is discussed. Further increase in boron content up to 5.6 % led to a strong increase in dislocation density, accompanied by a reduction in point defect density and formation of defect complexes. Surface morphology investigations revealed the formation of complex crystallites, as seen by scanning electron microscopy.

1. Introduction

Ternary BGaN materials have recently attracted considerable attention due to new opportunities for the lattice constant, bandgap, refractive index, strain, and polarization engineering [1]. Ideally, the introduction of boron would reduce the lattice mismatch with the underlying substrate, which, in turn, would reduce strain as well as the mismatch-related defect densities. A coherent lattice-matched interface for BGaN on AlN or SiC substrates could be achieved for boron content of 12 % or 17 %, respectively [2,3]. However, the development of BGaN-based devices has been stalled due to the difficulties in obtaining high-quality BGaN alloys and heterostructures, mainly due to the low solubility of boron in GaN [4,5]. *Ab initio* calculations [4] and thermodynamics considerations [5] indicated that B incorporation strongly depends on growth conditions and strain occurring in BGaN, and does not exceed only a few percent. Previous reports on BGaN growth have indicated the boron content of merely 3.6 % for BGaN layers grown on GaN/sapphire template [2,6–10]. Far higher B incorporation up to 15 % was demonstrated by using AlN/sapphire template [11–13,14]. Meanwhile, the maximum reported boron content was 5.6 % for the direct growth on SiC substrate [11].

The increasing boron content is, however, accompanied by worsening structural and optical quality of the layer. The structural analysis of BGaN layers revealed a high degree of mosaicity [15,16] with a drastic reduction of grain size for higher B content. The transformation of layer microstructure generated large densities of threading dislocations, despite the reduced lattice mismatch [15]. The formation of extended defects is also closely related to the formation of point defects, which might act as initiating centers for inversion layers and dislocations. It is generally thought that high extended defect concentrations are complemented with high vacancy concentrations, especially for high-temperature growth [17]. Recently, it has been argued that the increased growth temperature leads to the transfer of B atoms from Ga substitutional sites into the interstitial positions with the simultaneous

* Corresponding author.
** Corresponding author at: National Institute for Research and Development in Microtechnologies, Erou Iancu Nicolae 126A, Voluntari 077190, Romania
E-mail addresses: cosmin.romanitan@imt.ro (C. Romanitan), emil.pavelescu@imt.ro (E.M. Pavelescu).
[1] These authors contributed equally to this work.

https://doi.org/10.1016/j.jallcom.2025.184763
Received 2 September 2025; Received in revised form 16 October 2025; Accepted 29 October 2025
Available online 30 October 2025

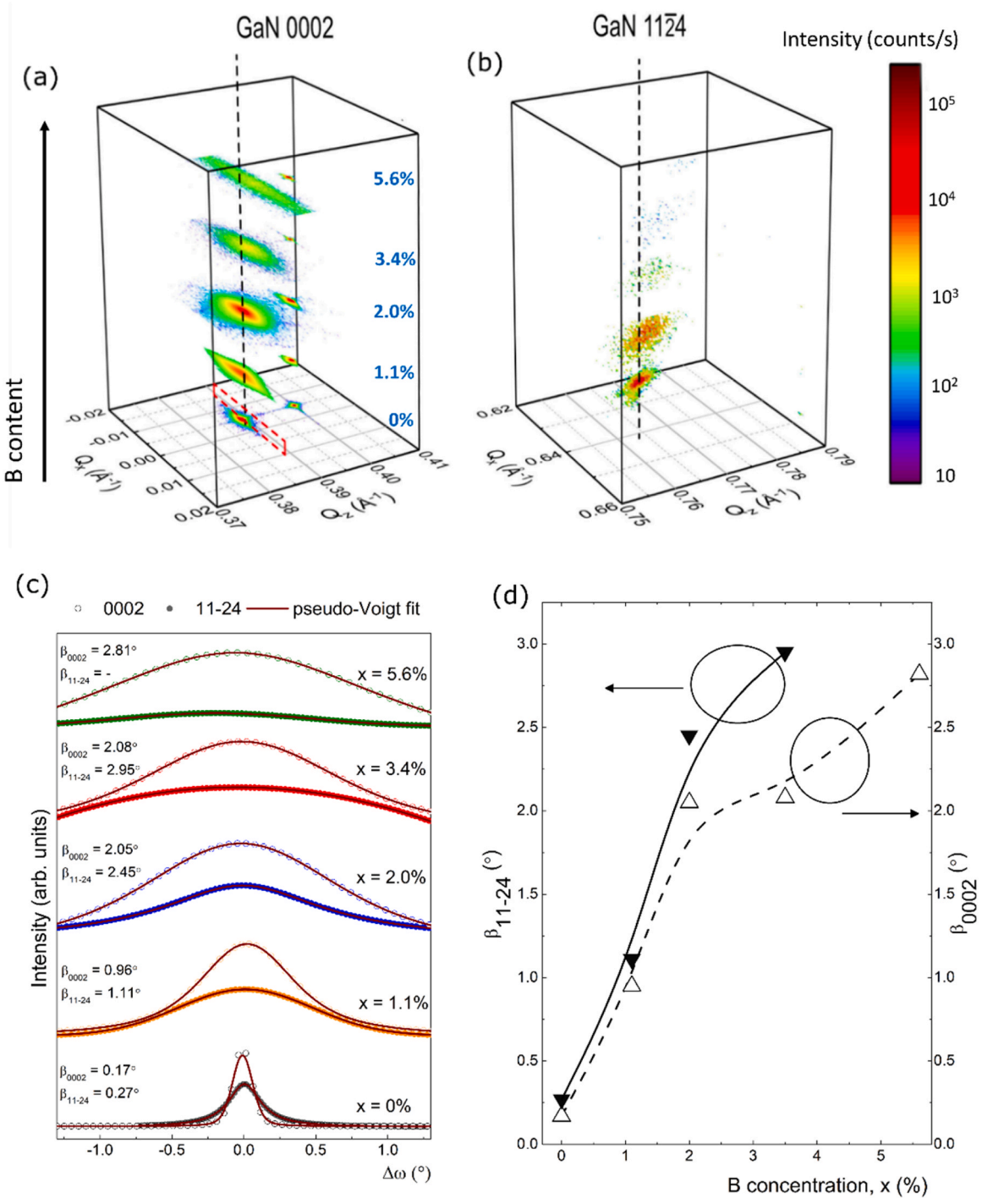

Fig. 1. RSM images in logarithmic scale of the studied BGaN layers with different boron content recorded around the 0002 (a) and 11$\bar{2}$4 (b) reflections. The RSM data are adopted from the ref. [15]. Vertical dashed lines indicate the positions of the GaN spot. (c) XRD Rocking curves obtained from the cross-sections of the reciprocal lattice spots, as highlighted with the dashed parallelogram in Fig. 1(a). Solid lines present the best fit using a pseudo-Voigt function. (d) Rocking curve width dependence on boron content.

creation of gallium vacancies [16,18]. Meanwhile, the large densities of dislocations and point defects resulted in quenching of the near-band-edge emission in favor of defect-related emission [16,19].

Thus, a fundamental understanding of the defect landscape in connection with the growth conditions is needed to exploit the full potential benefits of boron-containing nitride materials. Typically, either threading dislocation density or point defect concentration is analyzed in the literature, while considerably less attention is given to the interplay between the two types of defects [17,20–23]. In this work, we study the formation of the point defects in BGaN/SiC epitaxial layers with different boron content by using positron annihilation spectroscopy (PAS), and photoluminescence (PL) spectroscopy. Moreover, we discuss the relationship between point defects and dislocations and surface morphology by means of X-ray diffraction (XRD) and scanning electron microscopy (SEM). Our results show that the link between the extended and point defects should be analyzed considering the surface features of the layers.

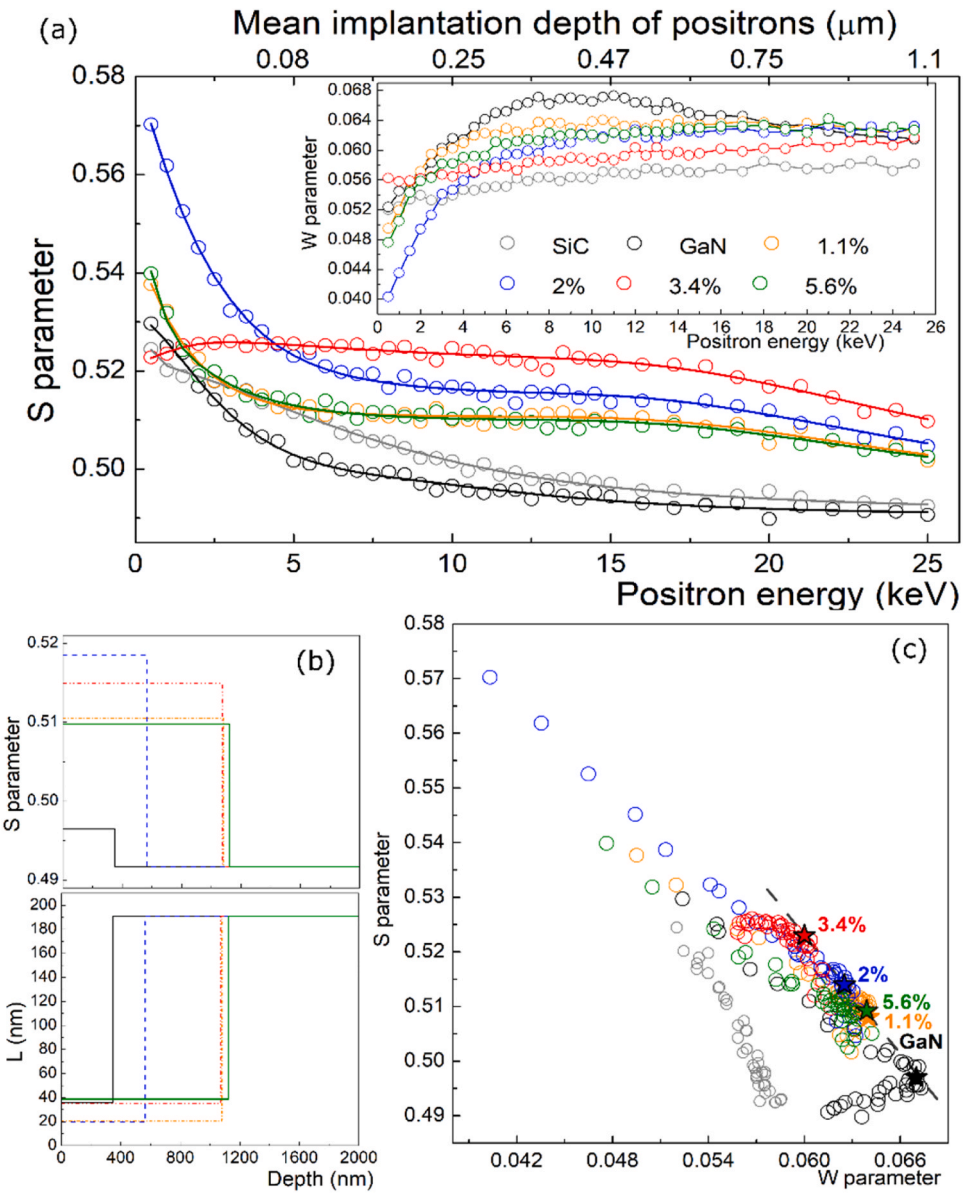

Fig. 2. (a) *S* parameter in the studied BGaN layers as a function of positron implantation energy. The inset presents the corresponding *W* parameter dependences. For comparison, data obtained in SiC substrate are also presented. Solid lines present the best fit using a two-layer model (see text for more details). (b) Depth distributions of *S* parameter and positron diffusion length *L* obtained from the fit. (c) (*S*, *W*) map of the studied samples. The stars indicate the characteristic points for the BGaN layers.

Table 1
Properties of the studied BGaN epilayers: boron content, *x*, mass density, ρ, epilayer thickness, *d*, *S* parameter, and the positron diffusion length, *L*. Data for the 6H-SiC substrate are also provided for comparison.

B content *x* (%)	Mass density ρ (g cm^{-3})	Layer thickness *d* (nm)	*S* parameter ± 0.0002	Positron diffusion length *L* (nm)
SiC	3.21	-	0.4917	191
0 (GaN)	6.15	348	0.4965	38
1.1	6.11	1080	0.5105	21
2.0	6.06	1073	0.5149	35
3.4	6.01	1230	0.5220	163
5.6	5.93	1124	0.5098	39

2. Experimental details

The BGaN layers were grown on 6H-SiC substrates by using metal-organic chemical vapor deposition (MOCVD) in a close-coupled showerhead 3 × 2" reactor (AIXTRON). The SiC substrates were used without any special nucleation or buffer layers, except for substrate annealing at 1050 °C before growth. More details related to the precursor flows and growth temperatures could be found in ref. [15]. Also, the high-resolution XRD setup used for recording the reciprocal space maps (RSMs) is described there.

Doppler broadening spectroscopy (DBS) measurements were performed at room temperature using the monoenergetic positron beam with adjustable energy of the Extreme Light Infrastructure Nuclear Physics (ELI-NP, IFIN-HH, Romania). Since the minimum dimension of the sample face was 5 mm, the positron beam was directed through a 3 mm aperture positioned at 70 cm distance from the sample, thus ensuring that the beam struck only the mounted sample. Two HPGe

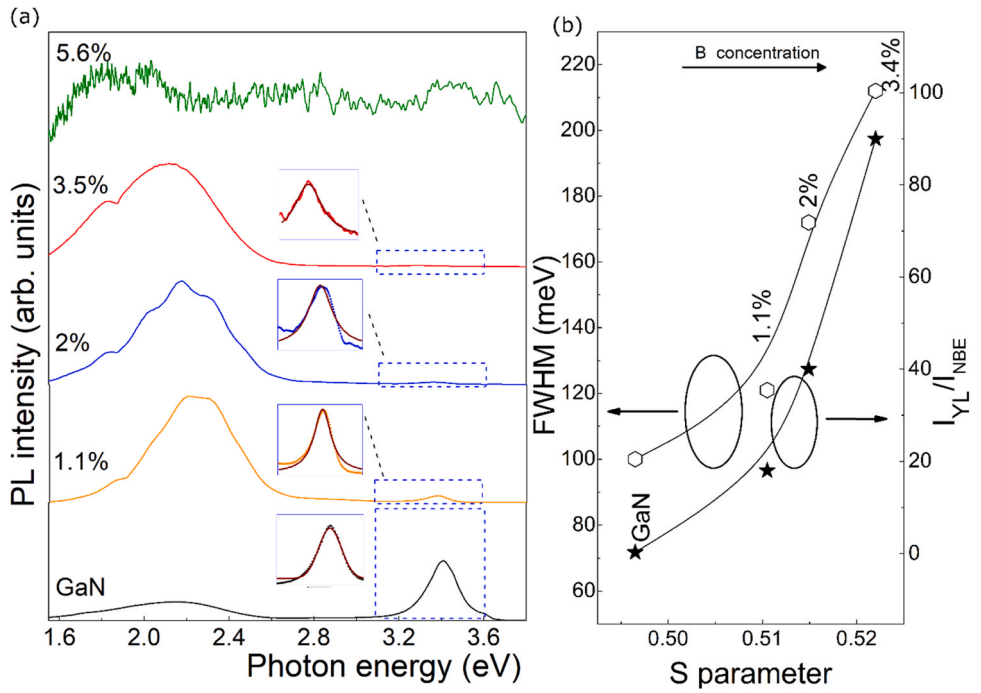

Fig. 3. (a) Room temperature PL spectra of the studied BGaN layers with different boron content (indicated). The insets present the expanded NBE region for clarity. (b) Correlation between the *S* parameter and the FWHM of the NBE band and the ratio between intensities of the YL and NBE bands.

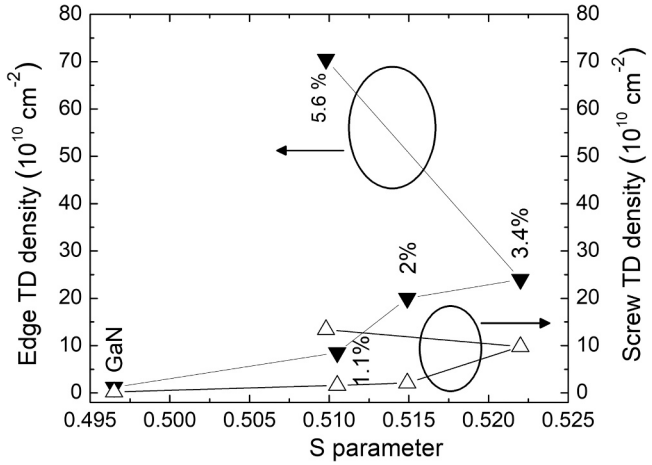

Fig. 4. Correlation between the *S* parameter and edge and screw TD density in the studied BGaN layers with different boron content (indicated).

detectors with 30 % efficiency and resolutions of 1.32 and 1.30 keV at 511 keV were positioned 8 cm from the samples, oriented perpendicularly to the beam axis. The detectors were shielded using 5-cm-thick lead to minimize the detection of annihilation gamma rays originating from the aperture walls. For each incident positron energy, *E*, in the range from 0.5 to 25 keV, spectra were acquired until approximately 5×10^5 counts were accumulated at the 511 keV peak. The Doppler broadening of the 511 keV annihilation line was analyzed using the common lineshape parameters: *S* was the fraction of annihilation events in the central part of the peak, representing annihilations with low-momentum electrons, while *W* was the fraction of annihilations with high-momentum electrons [24]. The averaged data from the two detectors was processed to extract the *S-E* dependences, further analyzed by VEPFIT software [25], which takes into account positron implantation, transport, trapping, and annihilation processes. The layer model, $S(E) = \sum_j S_j F_j(E)$, where $F_j(E)$ is the fraction of positrons annihilated in the j-th layer, and S_j is the characteristic parameter of the layer, was used to describe *S-E* curves.

SEM analysis was employed for the surface morphology study using a high-resolution field emission gun scanning electron microscope (FEI-NOVA NanoSEM 630) in top- and tilt-view at different magnifications.

PL spectra of the samples were measured at room temperature under steady-state excitation using the 4th harmonic (266 nm) of CW DPSS YAG:Nd laser radiation. The luminescence was collected in a front-surface configuration, analyzed by a monochromator, and detected by a UV-enhanced photomultiplier (Hamamatsu).

3. Results and discussions

Changes in the microstructure of BGaN layers due to the introduction of boron were studied by high-resolution XRD. RSM evolution with increasing B content is presented in Fig. 1(a) and (b) for the symmetric 0002 and asymmetric $11\bar{2}4$ reflections, respectively. The shift of the BGaN diffraction spot along Q_z towards the SiC reflection can be noticed in both geometries. As shown in more detail in our previous paper, the positions of BGaN spots allowed evaluation of the lattice constants $\boldsymbol{a}(\boldsymbol{BGaN})$using the equation (2) from ref. [15], and $\boldsymbol{c}(\boldsymbol{BGaN})$as $\boldsymbol{2/Q_z^{0002}}$. It was shown that$\boldsymbol{a}$ decreased from 3.194 to 3.180 Å, while $\boldsymbol{c}$decreased from 5.180 to 5.128 Å. The composition *x* in the $B_xGa_{1-x}N$ layers was calculated by applying the Vegard's law, and using the unstrained lattice parameters for wurtzite BN ($\boldsymbol{a(BN)} = 2.55$ Å and $\boldsymbol{c(BN)} = 4.17$ Å) taken from density functional calculation results [26]. The relative lattice mismatch at $B_xGa_{1-x}N$/SiC interface was evaluated as $\boldsymbol{m} = \frac{\boldsymbol{a(BGaN)}-\boldsymbol{a(SiC)}}{\boldsymbol{a(SiC)}}$, where $\boldsymbol{a(SiC)} = 3.073$ Å was determined using the positions of the SiC spots observed in the RSM distribution of the GaN/SiC epilayer. Thus, the increase in TEB/III ratio during growth from 1.7 % to 12.2 % resulted in the monotonous increase in the B content in the layer up to 5.6 % as well as in the decrease in the relative in-plane lattice mismatch from 3.9 % to 2.9 %, indicating growth with a lower mismatch at higher boron content [15]. Since strain relaxation in layers grown on lattice-mismatched substrates proceeds by the generation of misfit dislocations (MDs) at the interface and threading dislocations (TDs) in the

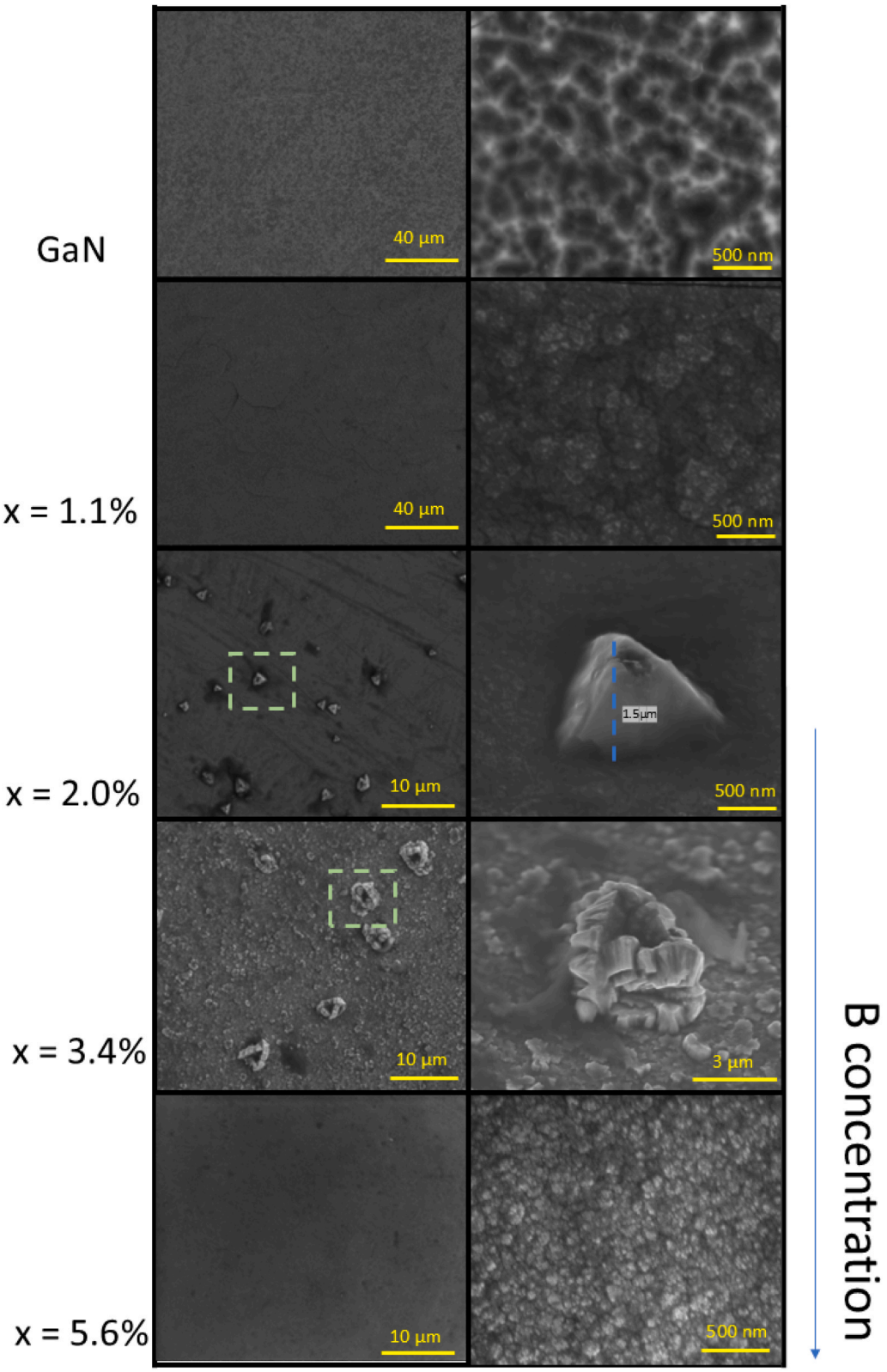

Fig. 5. Surface morphology images of the studied BGaN layers with different boron content (indicated) studied by SEM at different magnifications in top (left column) or tilt (right column) view.

bulk of the layer [27,28], the decreasing lattice mismatch between the BGaN layer and SiC substrate implies a lower density of misfit dislocations (MDs) in layers with higher B content. However, a large number of MDs and TDs is yet expected, since the BGaN layer thickness significantly exceeds the critical thickness even for the largest B content of our samples: both Matthews-Blakeslee [29] and Frank-der Merwe [30] models led to the critical thickness below 5 nm, while the thicknesses of our studied layers was ~ 1 µm.

Besides the position shift, the introduction of boron also caused the reciprocal lattice spot shape transformation: considerable broadening

and decrease in intensity, accompanied by the emergence of a strong diffuse scattering component, can be observed with increasing B content. The broad ellipsoidal reciprocal lattice spots indicate mosaic microstructure, while the observed shape transformation can be associated with the significant increase in threading dislocation (TD) densities [31]. The rocking curves of the 0002 (open points) and $11\bar{2}4$ (filled points) reflections obtained from the cross-sections of the respective reciprocal lattice spots (highlighted with red dashed parallelogram) are presented in Fig. 1(c). A pseudo-Voigt function was used to fit the experimental data, as illustrated by solid lines with the extracted FWHM values indicated next to each curve and plotted as a function of B content in Fig. 1(d). It is evident that the asymmetric $11\bar{2}4$ reflections result in the broader and less intense curves compared to the corresponding symmetric 0002 reflection, clearly indicating the predominance of edge TDs over screw TDs, consistent with the lower formation energy for the edge component [32]. For the reference GaN layer, the evaluated TD densities were 0.2×10^{10} and 1.2×10^{10} cm^{-2} of screw and edge TDs, respectively. A monotonous increase in TD densities with B content was observed, reaching 13.4×10^{10} and 70.5×10^{10} cm^{-2} of screw and edge TDs, respectively, in the BGaN layer with 5.6 % of boron [15]. Thus, contrary to the conventional framework of heteroepitaxy, where a smaller lattice mismatch typically leads to improved structural quality of the epilayer, BGaN epitaxy on SiC substrate instead favors the mosaic structure and the formation of high densities of TDs, despite the reduction in in-plane lattice mismatch.

To gain a better understanding of BGaN epitaxy, the point defects formed during the boron incorporation were studied using DBS with slow positron beam, one of the PAS techniques. Positron annihilation spectroscopy is an effective technique for the study of vacancy-type point defects in semiconductors [33]. Positrons implanted into material quickly thermalize and can get trapped in and localize at neutral and negative charged vacancies due to the missing positive ion core. Annihilation of a positron-electron pair produces two photons, each having an energy of ~511 keV. The component of the electron momentum parallel to the detection direction contributes to the Doppler broadening of the measured 511 keV line. In a defect-free material, the positron annihilates from a delocalized Bloch state, and the electron momentum distribution reflects the periodic lattice structure. However, in the presence of vacancies or negatively charged defects, the positron becomes trapped before annihilation, and the annihilation photons provide information about the electron momentum distribution at these trapping centers. PAS has been successfully applied to III-nitrides, revealing Ga vacancy and/or its complexe concentrations in the range of 10^{15}-10^{19} cm^{-3} in GaN bulk crystals and epilayers [17,34], and the defect distribution in GaN [35,36].

S and *W* parameter variations with positron energy for the SiC substrate are presented in Fig. 2(a). The top axis indicates the corresponding mean positron implantation depth, z_m, which depends on the positron energy through a simple empirical relation [37]: $z_m[nm] = (40/\rho) \times E^{1.62}[keV]$, where ρ is the mass density (in $g \cdot cm^{-3}$) of the probed material. The gradual decrease of the *S* parameter of the SiC substrate, with increasing positron energy, illustrates a characteristic long positron diffusion length. On the other hand, the saturation at energies above 15 keV of the *S* parameter value indicates that almost all positrons annihilate in the sample bulk. The observed *S*-*E* curve (see Fig. 2(a)) was fitted using a single-layer model. The obtained *S* parameter has a value of 0.4917. The positron diffusion length was evaluated to be 191 nm, which is typical for defect-free 6H-SiC [38–41].

For the $B_xGa_{1-x}N$ layers, it was assumed that the mass density varies linearly with B content, and the values used in calculations are provided in Table 1. *S*-*E* curves observed for nearly all the BGaN layers present a decrease in the *S* value from its initial surface value at low energies, to an almost constant value in the range of 7–15 keV, and then gradually decrease at higher energies. The gradual decrease in the *S* parameter above a certain implantation energy at around 12–16 keV indicates that positrons start penetrating and annihilating in the substrate. Therefore, a two-layer model was used to fit the experimental curves for the BGaN/SiC samples: the region probed by the positrons was divided into two blocks corresponding to the positron annihilation in the BGaN layer and SiC substrate. The values estimated for the SiC substrate, as discussed above, were set fixed in this model. Moreover, to keep the fitting model simple, the band bending near the surface or interface was neglected. The obtained fits are illustrated by solid lines in Fig. 2(a) with the derived depth distributions of *S* parameter and positron diffusion length shown in Fig. 2(b). All the obtained values are provided in Table 1. The evaluated BGaN layer thickness values are in good agreement with those estimated during the growth process. One can note that the positron diffusion length is relatively long (~163 nm) for the BGaN layer with 3.4 % of boron, which appears to contradict its high S parameter value, the highest among the studied BGaN layers. In our opinion, this discrepancy could be given by the presence of an internal electric field that is the strongest in this sample. This electric field at the interface could drive positrons back towards the surface, leading to a long positron diffusion length in the best-fit model. It is well known that the internal electric field is generated by a lot of factors, such as the difference in the work function in heterostructures, noncentrosymmetry or piezoelectricity [42,43]. Moreover, charges that accumulate at the surface of a nanomaterial due to defects or specific surface terminations can create a strong electric field. In particular, non-uniformity of the surface (e.g. columns, pyramids, rods etc.) could generate an additional internal electric field. As will be shown below, the surface of the BGaN layer with boron content of 3.4 % exhibits mutually interconnected crystallites of irregular shape. This distinctive surface morphology might contribute to the strongest internal electric field in that sample.

Almost in all the BGaN/SiC samples, the *S*(*W*) parameter of the epilayer is higher(lower) than that in the GaN/SiC sample (see Table 1), indicating the presence of additional vacancies in the grown epilayers with B-content. The nature of different vacancy-type positron traps in the material can be analyzed by using the *S*-*W* plot, presented in Fig. 2 (c). The characteristic (*S*, *W*) points of the BGaN layers form a straight line (shown by dashed line), which indicates that the defects in these layers are of the same type and only their concentration is different [44]. Since our studied GaN and BGaN layers are *n*-type, the most common native point defect is Ga vacancy (V_{Ga}) [45,46]. As the boron content in the layer increases up to 3.4 %, the *S* parameter increases from 0.4965 to 0.5220, which indicates increasing V_{Ga} concentration. Interestingly, the *S* parameter in BGaN layer with 5.6 % of B decreases down to a value comparable to that of the BGaN layer with 1.1 % of B, which indicates similar vacancy concentration as well. Similar nonmonotonous behavior of *S* parameter with doping was observed in Er-doped GaN, and was attributed to the degradation of crystallinity [47].

Ga vacancies are commonly associated with the yellow luminescence (YL) band in the PL spectrum of GaN [45,48]. Thus, the different concentrations of V_{Ga}, as indicated by the *S* parameter, should manifest in the different relative intensities of defect-related PL bands. The PL spectra of the studied BGaN layers are presented in Fig. 3(a). A strong near-band-edge (NBE) emission band at ~3.4 eV accompanied by a weak and broad YL band can be observed in the PL spectrum of GaN layer. Introduction of boron resulted in the drastic change of relative intensities of the two PL bands: the YL band became dominant, while the NBE band was hardly distinguishable. As the B content was increased, both YL and NBE bands systematically shifted to lower energies, while NBE band broadened and further decreased in intensity. The observed red shift of the NBE band could be understood in the framework of the local coherent potential approximation, which predicts a decrease in the band gap of BGaN alloys with increasing B content up to 20 % [49]. Meanwhile, the red shift of the YL band resembles the behavior previously reported for the deep-level related PL bands in InGaN materials with increasing In content [50]. This shift is associated with the radiative recombination mechanism responsible for the YL band in GaN, which is attributed to the distant donor–acceptor pair recombination

involving shallow donors and deep acceptors[45]. When GaN is alloyed with BN, the shallow donor level might be assumed to be linked to the conduction band edge (CBE), and hence it moves (downwards on a reference energy scale) together with the CBE when B content is increased, while the energy of the deep acceptor level is pinned at the same energy level (on the same reference scale) as the B concentration varies [51]. Consequently, the YL red shifts as the B content becomes larger. However, only weak emission with no discernible PL bands was measured for the BGaN layer with 5.6 % of boron. The drastic decrease in the NBE band intensity can be attributed to high densities of non-radiative recombination centers due to the increasing densities of both extended and point defects [3,15]. Meanwhile, the connection between Ga vacancies and YL band properties is further analyzed in Fig. 3(b), which presents the ratio between intensities of the YL and NBE bands (filled points) and FWHM of the YL band (open points) as functions of the *S* parameter. A clear correlation can be noticed, supporting the previously mentioned association.

To analyze the interplay between extended and point defects in the studied BGaN epilayers, the correlation between *S* parameter and TD densities is plotted in Fig. 4. Introduction of a small amount of boron (1.1 %) results in a significant increase in TD density accompanied by a considerable increase in vacancy concentration, as reflected by the increase of the *S* parameter. The simultaneous increase in both types of defects densities persists, although at a slower rate, with increase in boron content up to 3.4 %. Such correlation might indicate point defect clustering around the dislocations. Theoretical calculations suggested stable configurations of vacancies inside dislocation cores in GaN, and a correlation between vacancy densities and dislocations was established [21,22]. Enhanced formation of vacancy clusters was observed for the InN/GaN interface, and coincided with elevated dislocation densities in that area [20]. On the other hand, the increase in the *S* parameter might also be affected by the positron trapping at the shallow traps due to edge dislocations at the grain boundaries [23]. Meanwhile, the further increase in boron content to 5.6 % seems to result in lower point defect density, despite the increase in TD densities, and indicates either a significant degradation of the layer structural quality or additional factors affecting the *S* parameter value. A decrease in the *S* parameter despite an increase in the number of TDs could be understood if the increase in threading dislocations is accompanied by the formation of deeper trapping sites (like vacancy-jog complexes) [52] rather than large open-volume defects with low-momentum electrons, sensitive to the *S*-parameter. This is because the positrons are now preferentially annihilating at these deeper traps, which may have a different (higher) electron momentum distribution that results in a smaller *S*-parameter and a larger *W*-parameter, as observed in Fig. 2(c). The formation of these deeper traps could also explain the quenching of photoluminescence observed for the sample with the highest boron content.

Besides the internal microstructure of the BGaN layers reflected by the TDs, the positron trapping and annihilation could be affected by the surface features [53]. To analyze the impact of the surface in more detail, SEM micrographs at low (left column) and high magnifications (right column) were taken and are presented in Fig. 5. A smooth surface over a large area was observed for the GaN epilayer, while the zoomed-in picture revealed interconnected fibrils and dark pits due to the TD termination on the surface [54]. Introduction of boron at 1.1 % resulted in granular surface morphology with the typical grain size 700 nm, while the grains consisted of smaller crystallites with diameter of ~150 nm. For the BGaN layer with 2 % of B, the low magnification image indicates the presence of triangular crystallites with the density of $\sim 10^6$ cm^{-2}, while the magnified view of the object reveals the four-sided pyramidal hillock with height of 1.5 μm. Further increase in boron content to 3.4 % resulted in the appearance of large objects consisting of mutually interconnected irregular shapes crystallites on the surface. The crystallites seem to be embedded into the continuous layer. Meanwhile, the BGaN layer with the highest B content of 5.6 % exhibits a featureless smooth surface at low magnification, and the granular morphology at high magnification. This reversal of the morphology back to the smooth surface could also be responsible for the observed lower S parameter. The results strongly suggest that the formed crystallite clusters on the surface might act as the additional source of Ga-vacancies in the layers.

4. Conclusions

We have studied the interplay between extended and point defects in BGaN epilayers grown on SiC. XRD measurements revealed the mosaic structure of the layers with high threading dislocation densities, that increase with boron content. The Doppler broadening of the 511 keV annihilation line indicated that the introduction of B atoms promoted the formation of additional point defects, most likely V_{Ga}, which was confirmed by the increase in the relative intensity of YL band. Meanwhile, the drastic decrease in the NBE band was associated with high densities of nonradiative recombination centers. A clear correlation between extended and point defects was observed for boron content up to 3.4 % suggesting point defect clustering around dislocations. Formation of complex crystallites on the surface was indicated as the source of extra defects in the layers. Meanwhile, the correlation ceased for higher boron content of 5.6 % indicating additional factors affecting the structural quality, most likely by formation of defect complexes which act as deep traps for carriers. The presented results on BGaN ternary alloys are important for the further development of B-containing nitride materials grown on various substrates.

Funding sources

This research was financed by the Romanian Core Program PNCDI 2022–2027, "Cercetari avansate in dispozitive micronano-electronice, fotonice, senzori si microsisteme pentru aplicatii societale – μNanoEl" code, financed by the Ministry of Research, Innovation and Digitalization. N.D. and A.B.S. acknowledge the support by PN 23.21.01.06 sponsored by the Romanian Ministry of Research, Innovation, and Digitization. C.R. and E.M.P also acknowledge the support by the project ELI-RO_19 "HighProtonPLas" funded by IFA. The research at Vilnius University has been carried out in the framework of the "Universities` Excellence Initiative" program by the Ministry of Education, Science and Sports of the Republic of Lithuania under the agreement with the Research Council of Lithuania (project No. S-A-UEI-23–6).

Declaration of Competing Interest

The authors declare that they have no known competing financial interests or personal relationships that could have appeared to influence the work reported in this paper.

References

[1] R. Kudrawiec, D. Hommel, Bandgap engineering in III-nitrides with boron and group v elements: toward applications in ultraviolet emitters, Appl. Phys. Rev. 7 (2020) 041314, https://doi.org/10.1063/5.0025371.
[2] A. Ougazzaden, S. Gautier, C. Sartel, N. Maloufi, J. Martin, F. Jomard, BGaN materials on GaN/sapphire substrate by MOVPE using N2 carrier gas, J. Cryst. Growth 298 (2007) 316–319, https://doi.org/10.1016/j.jcrysgro.2006.10.072.
[3] J. Jurkevičius, J. Mickevičius, A. Kadys, M. Kolenda, G. Tamulaitis, Photoluminescence efficiency of BGaN epitaxial layers with high boron content, Phys. B Condens. Matter 492 (2016) 23–26, https://doi.org/10.1016/j.physb.2016.03.033.
[4] L. Lymperakis, Ab-initio study of boron incorporation and compositional limits at GaN and AlN (0001) surfaces, AIP Adv. 8 (2018) 065301, https://doi.org/10.1063/1.5029339.
[5] J.X. Shen, M.E. Turiansky, D. Wickramaratne, C.G. Van De Walle, Thermodynamics of boron incorporation in BGaN, Phys. Rev. Mater. 5 (2021) 065001, https://doi.org/10.1103/PhysRevMaterials.5.L030401.
[6] G. Orsal, N. Maloufi, S. Gautier, M. Alnot, A. Sirenko, G. Orsal, N. Maloufi, S. Gautier, M. Alnot, A. Sirenko, M. Journal, G. Orsal, N. Maloufi, S. Gautier, M. Alnot, A.A. Sirenko, M. Bouchaour, A. Ougazzaden, Effect of boron incorporation on growth behavior of BGaN / GaN by MOVPE, J. Cryst. Growth 310 (2008) 5058–5062.

[7] S. Gautier, G. Patriarche, T. Moudakir, M. Abid, G. Orsal, K. Pantzas, D.D. Troadec, A. Soltani, L. Largeau, O. Mauguin, A. Ougazzaden, Deep structural analysis of novel BGaN material layers grown by MOVPE, J. Cryst. Growth 315 (2011) 288–291, https://doi.org/10.1016/j.jcrysgro.2010.08.042.

[8] K. Atsumi, Y. Inoue, H. Mimura, T. Aoki, T. Nakano, Neutron detection using boron gallium nitride semiconductor material, APL Mater. 2 (2014) 032106, https://doi.org/10.1063/1.4868176.

[9] T. Malinauskas, A. Kadys, S. Stanionyte, K. Badokas, J. Mickevičius, J. Jurkevičius, D. Dobrovolskas, G. Tamulaitis, Growth of BGaN epitaxial layers using close-coupled showerhead MOCVD, Phys. Status Solidi 252 (2015) 1138–1141, https://doi.org/10.1002/pssb.201451560.

[10] R.C. Cramer, B. Bonef, J. English, C.E. Dreyer, C.G. Van de Walle, J.S. Speck, Growth of coherent BGaN films using BBr3 gas as a boron source in plasma assisted molecular beam epitaxy, J. Vac. Sci. Technol. A Vac. Surf. Film. 35 (2017) 041509, https://doi.org/10.1116/1.4986185.

[11] A. Kadys, J. Mickevičius, T. Malinauskas, J. Jurkevičius, M. Kolenda, S. Stanionyte, D. Dobrovolskas, G. Tamulaitis, Optical and structural properties of BGaN layers grown on different substrates, J. Phys. D. Appl. Phys. 48 (2015) 465307, https://doi.org/10.1088/0022-3727/48/46/465307.

[12] B.P. Gunning, M.W. Moseley, D.D. Koleske, A.A. Allerman, S.R. Lee, Phase degradation in BxGa1−xN films grown at low temperature by metalorganic vapor phase epitaxy, J. Cryst. Growth 464 (2017) 190–196, https://doi.org/10.1016/j.jcrysgro.2016.10.054.

[13] M.A. Rather, L. Ravi, T.Y. Yu, C.T. Wu, K.L. Lin, K.Y. Lai, J.I. Chyi, An experimental study of the energy band alignments of B(Al, Ga)N heterojunctions, Appl. Phys. Lett. 123 (2023) 012101, https://doi.org/10.1063/5.0116951.

[14] F. Alqatari, M. Sajjad, R. Lin, K.-H. Li, U. Schwingenschlögl, X. Li, Optical properties of BAlN and BGaN for applications in lattice-matched UV optical structures, Arxiv. (n.d.). https://doi.org/10.48550/arXiv.1803.10011.

[15] C. Romanitan, J. Mickevičius, F. Comanescu, R. Gavrila, M. Stoian, P. Varasteanu, A. Kadys, T. Malinauskas, E.M. Pavelescu, The effects of low boron incorporation on the structural and optical properties of BxGa1-xN/SiC epitaxial layers, J. Appl. Crystallogr 57 (2024) 1815–1822, https://doi.org/10.1107/S1600576724009579.

[16] E.B. Możdżyńska, P. Kamiński, R. Kozłowski, K.P. Korona, S. Złotnik, E. Jezierska, J.M. Baranowski, Effect of the growth temperature on the formation of deep-level defects and optical properties of epitaxial BGaN, J. Mater. Sci. 57 (2022) 17347–17362, https://doi.org/10.1007/s10853-022-07725-4.

[17] F. Tuomisto, J.M. Mäki, C. Rauch, I. Makkonen, On the formation of vacancy defects in III-nitride semiconductors, J. Cryst. Growth 350 (2012) 93–97, https://doi.org/10.1016/j.jcrysgro.2011.12.031.

[18] J. Kierdaszuk, E.B. Możdżynska, A. Drabińska, A. Wysmolek, J.M. Baranowski, Electron paramagnetic resonance of VN–VGa complex in BGaN, APL Mater. 11 (2023) 101119, https://doi.org/10.1063/5.0153522.

[19] E. Zdanowicz, D. Iida, L. Pawlaczyk, J. Serafinczuk, R. Szukiewicz, R. Kudrawiec, D. Hommel, K. Ohkawa, Boron influence on bandgap and photoluminescence in BGaN grown on AlN, J. Appl. Phys. 127 (2020) 165703, https://doi.org/10.1063/1.5140413.

[20] C. Rauch, F. Tuomisto, A. Vilalta-Clemente, B. Lacroix, P. Ruterana, S. Kraeusel, B. Hourahine, W.J. Schaff, Defect evolution and interplay in n-type InN, Appl. Phys. Lett. 100 (2012) 091907, https://doi.org/10.1063/1.3688038.

[21] S. Kraeusel, B. Hourahine, Global search for stable screw dislocation cores in III-N semiconductors, Phys. Status Solidi 209 (2012) 71–74, https://doi.org/10.1002/pssa.201100097.

[22] J. Oila, J. Kivioja, V. Ranki, K. Saarinen, D.C. Look, R.J. Molnar, S.S. Park, S.K. Lee, J.Y. Han, Ga vacancies as dominant intrinsic acceptors in GaN grown by hydride vapor phase epitaxy, Appl. Phys. Lett. 82 (2003) 3433–3435, https://doi.org/10.1063/1.1569414.

[23] J. Oila, K. Saarinen, A.E. Wickenden, D.D. Koleske, R.L. Henry, M.E. Twigg, Ga vacancies and grain boundaries in GaN, Appl. Phys. Lett. 82 (2003) 1021–1023, https://doi.org/10.1063/1.1542946.

[24] I. Makkonen, F. Tuomisto, Perspective on defect characterization in semiconductors by positron annihilation spectroscopy, J. Appl. Phys. 135 (2024) 040901, https://doi.org/10.1063/5.0180024.

[25] A. van Veen, H. Schut, J. de Vries, R.A. Hakvoort, M.R. Ijpma, Analysis of positron profiling data by means of "VEPFIT, AIP Conf. Proc. 218 (1991) 171–198, https://doi.org/10.1063/1.40182.

[26] C.E. Dreyer, J.L. Lyons, A. Janotti, C.G. Van De Walle, Band alignments and polarization properties of BN polymorphs, Appl. Phys. Express 7 (2014) 031001, https://doi.org/10.1039/d0tc01578d.

[27] V.M. Kaganer, O. Brandt, A. Trampert, K.H. Ploog, X-ray diffraction peak profiles from threading dislocations in GaN epitaxial films, Phys. Rev. B Condens. Matter Mater. Phys. 72 (2005) 045423, https://doi.org/10.1103/PhysRevB.72.045423.

[28] V.M. Kaganer, X-ray diffraction from dislocation half-loops in epitaxial films, J. Appl. Crystallogr 57 (2024) 276–283, https://doi.org/10.1107/S160057672400089X.

[29] J.W. Matthews, A.E. Blakeslee, Defects in epitaxial multilayers, J. Cryst. Growth 27 (1974) 118–125, https://doi.org/10.1016/S0022-0248(74)80055-2.

[30] J.H. Van Der Merwe, Crystal Interfaces. Part II. Finite Overgrowths, J. Appl. Phys. 34 (1963) 123–127, https://doi.org/10.1063/1.1729051.

[31] R. Chierchia, T. Böttcher, H. Heinke, S. Einfeldt, S. Figge, D. Hommel, Microstructure of heteroepitaxial GaN revealed by x-ray diffraction, J. Appl. Phys. 93 (2003) 8918–8925, https://doi.org/10.1063/1.1571217.

[32] S.K. Mathis, A.E. Romanov, L.F. Chen, G.E. Beltz, W. Pompe, J.S. Speck, Modeling of threading dislocation reduction in growing GaN layers, J. Cryst. Growth 231 (2001) 371–390.

[33] F. Tuomisto, I. Makkonen, Defect identification in semiconductors with positron annihilation: Experiment and theory, Rev. Mod. Phys. 85 (2013) 1583–1631, https://doi.org/10.1103/RevModPhys.85.1583.

[34] K. Saarinen, T. Laine, S. Kuisma, J. Nissila, P. Hautojarvi, L. Dobrzynski, J. M. Baranowski, K. Pakula, R. Stepniewski, M. Wojdak, A. Wysmolek, T. Suski, M. Leszczynski, I. Grzegory, S. Porowski, Observation of native Ga vacancies in GaN by positron annihilation, Phys. Rev. Lett. 482 (1997) 757–762, https://doi.org/10.1557/proc-482-757.

[35] P. Rice-Evans, A.S. Saleh, M. Nathwani, J.W. Taylor, C.T. Foxon, Positron studies of MBE-grown gallium nitride, Appl. Surf. Sci. 149 (1999) 165–169, https://doi.org/10.1016/S0169-4332(99)00194-4.

[36] F. Tuomisto, T. Paskova, R. Kröger, S. Figge, D. Hommel, B. Monemar, R. Kersting, Defect distribution in a-plane GaN on Al2O3, Appl. Phys. Lett. 90 (2007) 121915, https://doi.org/10.1063/1.2715128.

[37] A. Vehanen, K. Saarinen, P. Hautojärvi, H. Huomo, Profiling multilayer structures with monoenergetic positrons, Phys. Rev. B. 35 (1987) 4606–4610, https://doi.org/10.1103/PhysRevB.35.4606.

[38] H. Wang, H. Weng, X. Zhou, Defect Characterization of 6H-SiC Studied by Slow Positron Beam, Chin. J. Chem. Phys. 21 (2008) 333–338, https://doi.org/10.1088/1674-0068/21/04/333-338.

[39] M.-F. Barthe, L. Henry, C. Corbel, G. Blondiaux, K. Saarinen, P. Hautojärvi, E. Hugonnard, L. Di Cioccio, F. Letertre, B. Ghyselen, Positron annihilation at proton-induced defects in 6H-SiC/SiC and 6H-SiC/SiO2/Si structures, Phys. Rev. B. 62 (2000) 16638–16644, https://doi.org/10.1103/PhysRevB.62.16638.

[40] A. Kawasuso, F. Redmann, R. Krause-Rehberg, T. Frank, M. Weidner, G. Pensl, P. Sperr, H. Itoh, Vacancies and deep levels in electron-irradiated 6H SiC epilayers studied by positron annihilation and deep level transient spectroscopy, J. Appl. Phys. 90 (2001) 3377–3382, https://doi.org/10.1063/1.1402144.

[41] G.P. Karwasz, R. Rurali, G. Consolati, P. Godignon, Defect dynamics in P + implanted 6H -SiC studied by positron annihilation spectroscopy, Phys. Status Solidi 1 (2004) 257–260, https://doi.org/10.1002/pssc.200303939.

[42] A. Gautam, A. Rameshwari, S.K. Das, Internal Electric Field Developed at the Interface between CoNiP Core and ZnIn 2 S 4 Shell Leading to Efficient Charge Separation for Photochemical Hydrogen Evolution, ACS Appl. Nano Mater. 8 (2025) 17886–17899, https://doi.org/10.1021/acsanm.5c02699.

[43] L. Chen, J. Ren, Z. Yuan, Enabling Internal Electric Fields to Enhance Energy and Environmental Catalysis, Adv. Energy Mater. 13 (2023) 2203720, https://doi.org/10.1002/aenm.202203720.

[44] A. Pelli, K. Saarinen, F. Tuomisto, S. Ruffenach, O. Briot, Influence of V/III molar ratio on the formation of in vacancies in InN grown by metal-organic vapor-phase epitaxy, Appl. Phys. Lett. 89 (2006) 10–13, https://doi.org/10.1063/1.2219335.

[45] M.A. Reshchikov, H. Morkę, Luminescence properties of defects in GaN, J. Appl. Phys. 97 (2005) 061301, https://doi.org/10.1063/1.1868059.

[46] M.A. Reshchikov, A. Usikov, H. Helava, Y. Makarov, V. Prozheeva, I. Makkonen, F. Tuomisto, J.H. Leach, K. Udwary, Evaluation of the concentration of point defects in GaN, Sci. Rep. 7 (2017) 9297, https://doi.org/10.1038/s41598-017-08570-1.

[47] A. Uedono, C. Shaoqiang, S. Jongwon, K. Ito, H. Nakamori, N. Honda, S. Tomita, K. Akimoto, H. Kudo, S. Ishibashi, Vacancy-type defects in Er-doped GaN studied by a monoenergetic positron beam, J. Appl. Phys. 103 (2008) 104505, https://doi.org/10.1063/1.2932166.

[48] Q.J. Wang, H.S. Zhang, L. Shi, J. Gong, Origin of Ga vacancy-related YL center in n-type GaN: A first-principles study, J. Lumin 255 (2023) 119561, https://doi.org/10.1016/j.jlumin.2022.119561.

[49] A. Ougazzaden, S. Gautier, T. Moudakir, Z. Djebbour, Z. Lochner, S. Choi, H.J. Kim, J.H. Ryou, R.D. Dupuis, A.A. Sirenko, Bandgap bowing in BGaN thin films, Appl. Phys. Lett. 93 (2008) 083118, https://doi.org/10.1063/1.2977588.

[50] C. Manz, M. Kunzer, H. Obloh, A. Ramakrishnan, U. Kaufmann, In x Ga 1−x N/GaN band offsets as inferred from the deep, yellow-red emission band in InxGa1−xN, Appl. Phys. Lett. 74 (1999) 3993–3995, https://doi.org/10.1063/1.124247.

[51] J. Mickevičius, M. Andrulevicius, O. Ligor, A. Kadys, R. Tomašiūnas, G. Tamulaitis, E.-M. Pavelescu, Type-II band alignment of low-boron-content BGaN/GaN heterostructures, J. Phys. D. Appl. Phys. 52 (2019) 325105, https://doi.org/10.1088/1361-6463/ab2337.

[52] L.C. Smedskjaer, M. Manninen, M.J. Fluss, An alternative interpretation of positron annihilation in dislocations, J. Phys. F. Met. Phys. 10 (1980) 2237–2249, https://doi.org/10.1088/0305-4608/10/10/019.

[53] X.D. Pi, P.G. Coleman, C.L. Tseng, C.P. Burrows, B. Yavich, W.N. Wang, Defects in GaN films studied by positron annihilation spectroscopy, J. Phys. Condens. Matter 14 (2002) L243, https://doi.org/10.1088/0953-8984/14/12/102.

[54] C. Romanitan, R. Gavrila, M. Danila, Comparative study of threading dislocations in GaN epitaxial layers by nondestructive methods, Mater. Sci. Semicond. Process 57 (2017) 32–38, https://doi.org/10.1016/j.mssp.2016.09.021.